

Strong-Weak Distribution Alignment for Adaptive Object Detection

Kuniaki Saito¹ Yoshitaka Ushiku² Tatsuya Harada^{2,3} Kate Saenko¹

¹Boston University, ²The University of Tokyo, ³RIKEN

¹{keisaito, saenko}@bu.edu, ²{ushiku, harada}@mi.t.u-tokyo.ac.jp

Abstract

We propose an approach for unsupervised adaptation of object detectors from label-rich to label-poor domains which can significantly reduce annotation costs associated with detection. Recently, approaches that align distributions of source and target images using an adversarial loss have been proven effective for adapting object classifiers. However, for object detection, fully matching the entire distributions of source and target images to each other at the global image level may fail, as domains could have distinct scene layouts and different combinations of objects. On the other hand, strong matching of local features such as texture and color makes sense, as it does not change category level semantics. This motivates us to propose a novel approach for detector adaptation based on strong local alignment and weak global alignment. Our key contribution is the weak alignment model, which focuses the adversarial alignment loss on images that are globally similar and puts less emphasis on aligning images that are globally dissimilar. Additionally, we design the strong domain alignment model to only look at local receptive fields of the feature map. We empirically verify the effectiveness of our approach on several detection datasets comprising both large and small domain shifts.

1. Introduction

Deep convolutional neural networks have greatly improved object recognition accuracy [18], but remain reliant on large quantities of labeled training data. For object detection, annotation is particularly burdensome: each instance of an object category in every image must be annotated with a precise bounding box. Transferring pre-trained models from label-rich domains is an attractive solution, but dataset bias often reduces their generalization to novel data [31].

Various methods for unsupervised domain adaptation (UDA) have been proposed to tackle the dataset bias problem [10, 40, 39, 25], most of which are based on domain-invariant alignment of the feature [32] or image [21, 14] distributions. Recent methods align the source and target

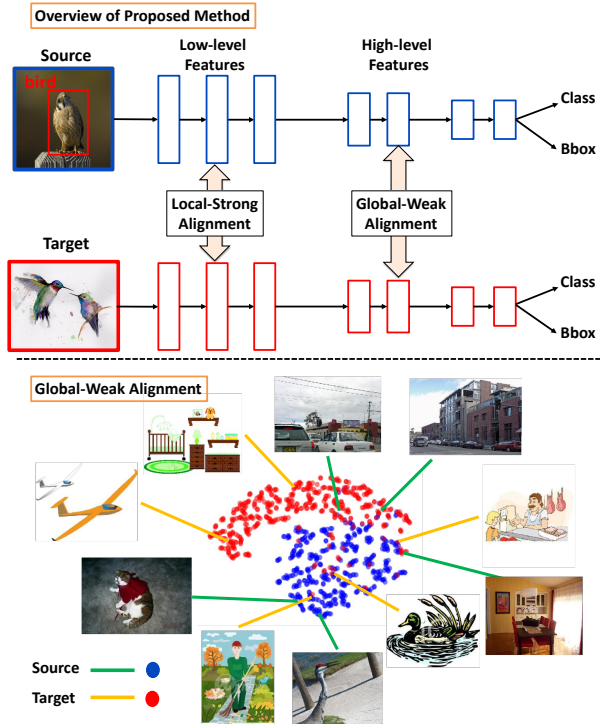


Figure 1. Upper: Our Strong-Weak model learns domain-invariant features that are strongly aligned at the local patch level and weakly (partially) aligned at the global scene level. Lower: Global features obtained by our proposed weak alignment method. The target features are partially aligned with source, which improves detection performance, as shown in our experiments.

distributions of examples using adversarial learning and are motivated by theoretical results that bound the generalization error partially by the size of the discrepancy between domains [2, 1]. The conventional wisdom is therefore that discrepancy must be reduced at all costs, which can only be done if one fully aligns the distributions. In this paper, we argue that such *strong* domain alignment is only reasonable in closed problems, such as object classification settings where the source and target examples share the same categories and prior label distributions. In settings such as open-set classification [4] or partial domain adaptation [41],

strong alignment can be infeasible and could actually hurt performance.

In object detection this is particularly evident, as aligning global (image-level) features means that not only the object categories, but also backgrounds and scene layouts must be similar across domains. Yet this is precisely what the current state-of-the-art UDA method for detection, Adaptive Faster RCNN [5], attempts to do. It modifies the Faster RCNN architecture to include a domain classifier trained to distinguish source and target examples, while the feature extractor learns to deceive the domain classifier. Feature alignment is done both at the global image scale and at the instance (object) scale.

While the global matching might work well for small domain shifts that only affect the appearance/textured of objects (e.g. weather related shifts), it is likely to hurt performance for larger shifts that affect the layout of the scene, the number of objects and/or their co-occurrence. For example, source images may contain single objects, while target images may contain multiple smaller objects. Forcing invariance to such *global* features can remove information required for object detection. On the other hand, strong alignment of *local* features would match the texture or color of the domains and should improve performance, because it will not change the category information but is likely to reduce the domain gap. In this paper, by “local” scale we do not mean the instance (object) scale but rather texture or color.

Motivated by these observations, we propose an unsupervised adaptation method for object detection that combines *weak global* alignment with *strong local* alignment, called the Strong-Weak Domain Alignment model (top of Fig. 1). We propose to apply *weak* alignment to the *global* features, partially aligning them to reduce the domain gap without hurting the performance of the model. We show an example of weak global alignment in the bottom of Fig. 1, where only the target images which contain one object are aligned with the source, whereas most target images are not aligned with the source. Our key contribution is the weak global alignment model, which focuses the adversarial alignment loss toward images that are globally similar, and away from images that are globally dissimilar. Additionally, we achieve strong local alignment by constructing another domain classifier designed to look only at local features and to strictly align them with the other domain. We verify the effectiveness of our method both in adaptation between similar and dissimilar domains.

2. Related Work

Object Detection. The development of deep convolutional neural networks has boosted the performance of object detection. Having a strong backbone feature extractor is key for accurate detection models. Current detection networks

can be categorized into two types: two-stage and one-stage. Faster-RCNN (FRCNN) [30] is a representative two-stage detector that generates coarse object proposals using region proposal networks (RPN) as the first stage, and feeds the proposals and cropped features into a classification module as the second stage. In this paper, we use the FRCNN as a base detector, however, our method should be applicable to other two-stage detectors and one-stage detectors such as YOLO [29] or SSD [22]. Detector back-bone networks are usually pre-trained on ImageNet [7] and need to be fine-tuned again with a large number of annotated object bounding boxes. Various datasets have been publicized for this purpose [8, 7, 20]. To deal with the deficit in such large annotated datasets, weakly supervised and semi-supervised object detection has been proposed in the literature [38, 3]. Although cross-domain object detection and especially unsupervised cross-domain object detection can also help with this problem, as far as we know, there is only one work that has tackled the task of unsupervised domain transfer of deep object detectors [5]. In this work, the feature alignment at the instance (object) scale was done for features cropped by region proposals. To effectively conduct feature alignment, region proposals have to precisely localize objects of interest. However, this is difficult to do for the target domain as we are not given ground truth proposals. The feature alignment may therefore hurt the performance of the model as we show in our experiments, which is why we do not conduct instance scale alignment in our work.

Domain Adaptation. The problem of bridging a gap between domains has been investigated for various visual applications such as image classification and semantic segmentation [31, 40, 43, 35].

To solve the problem, a large number of methods utilize feature distribution matching between training and testing domains. The basic idea is to measure some type of distance between different domains’ feature distributions and train a feature extractor to minimize that distance. Various ways of measuring the distance have been proposed [9, 40, 39, 23, 25, 33]. Motivated by a theoretical result [2, 1], various approaches utilize the domain classifier [9, 40, 39] to measure domain discrepancy. They train a domain classifier and feature extractor in an adversarial way, as done for training GANs [11]. Such methods are designed to strictly align the feature distribution of the target with that of the source. In addition, Long *et al.* designed a loss function of the domain classifier to strictly match features between domains [24] for image classification.

In this paper, we instead propose a weak feature alignment model for global features, and use strong alignment only at the local level to strictly align the style of images across domains. Some research on GANs and domain adaptive semantic segmentation has shown that regularizing the domain classifier with task-specific classification loss can

stabilize the adversarial training [27, 35]. Motivated by this approach, we further propose a method to regularize the domain classifier by the detection loss on source examples.

3. Method

The architecture of our proposed Strong-Weak DA model is illustrated in Fig. 3. We extract global features just before the RPN and local features from lower layers, and perform *weak global* alignment in the high-level feature space and *strong local* alignment in the low-level feature space. We further propose to stabilize the training of domain classifiers with the detection loss (Sec. 3.3).

3.1. Weak Global Feature Alignment

We utilize a domain classifier to align the target features with the source for the global-level feature alignment. Easy-to-classify target examples are located far from source examples in the feature space while hard-to-classify target examples are near the source as shown in the left of Fig. 2. Therefore, focusing on hard-to-classify examples should achieve a weak alignment between domains. We propose to train a domain classifier to ignore easy-to-classify examples while focusing on hard-to-classify examples with respect to the classification of the domain.

We have access to a labeled source image x^s and bounding boxes for each image y^s drawn from a set of annotated source images $\{X_s, Y_s\}$, as well as an unlabeled target image x^t drawn from unlabeled target images X_t . The global feature vector is extracted by F . The domain classifier, D_g , is trained to predict the domain of input global features. Our learning formulation optimizes F so that the features are discriminative for the primary task of object detection, but are uninformative for the task of domain classification. The domain-label d is 1 for the source and 0 for the target. The network R takes features from F and outputs bounding boxes with a class label. R includes the Region Proposal Network (RPN) and other modules in Faster RCNN. The objective of the detection loss is summarized as:

$$\mathcal{L}_{cls}(F, R) = -\frac{1}{n_s} \sum_{i=1}^{n_s} \mathcal{L}_{det}(R(F(x_i^s)), y_i^s) \quad (1)$$

where we assume that \mathcal{L}_{det} contains all losses for detection such as a classification loss and a bounding-box regression loss. n_s denotes the number of source examples.

In existing methods [5], the objective for domain classification is the cross-entropy loss. As shown in Fig. 2, the loss of the easy-to-classify examples, which have high probability, is not negligible in this cross-entropy loss. This indicates that D_g and F account for all examples in the training procedure. Therefore, F tries to match the entire feature distribution, which is not desirable in domain adaptive object detection.

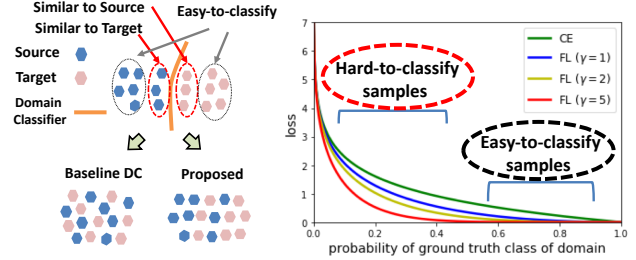


Figure 2. Left: Weak-distribution alignment using a domain classifier. Right: Standard cross-entropy loss and focal loss.

Instead, we want the domain classifier to ignore easy-to-classify examples while focusing on hard-to-classify examples. The problem with cross-entropy (CE) loss ($-\log p$) is that it puts non-negligible values of easy-to-classify examples where $p \in [0, 1]$ is the model's estimated probability for the class with label $d = 1$. We propose to add a modulating factor $f(p_t)$ to the cross-entropy loss, resulting in

$$-f(p_t) \log(p_t) \quad (2)$$

where we define p_t :

$$p_t = \begin{cases} p & \text{if } d = 1 \\ 1 - p & \text{otherwise.} \end{cases} \quad (3)$$

We choose a function that decreases as p_t increases. One example of such a loss function is Focal Loss (FL) [19]

$$FL(p_t) = -f(p_t) \log(p_t), f(p_t) = (1 - p_t)^\gamma \quad (4)$$

where γ controls the weight on hard-to-classify examples. FL is designed to put more weight on hard-to-classify examples than on easy ones during training, as shown in the right of Fig. 2. The feature extractor tries to deceive the domain classifier, that is, tries to increase the loss. However, the feature extractor cannot align the well-classified target examples with the source because the scale of gradients of such examples is very small. The same can be said about aligning source examples to the target. $f(p_t)$ can take other formulations if it satisfies the requirement described above. In experiments, we will show the result of another loss function that satisfies the condition. We denote the loss of the weak global-level domain classifier as \mathcal{L}_{global} as follows,

$$\mathcal{L}_{global_s} = -\frac{1}{n_s} \sum_{i=1}^{n_s} (1 - D_g(F(x_i^s)))^\gamma \log(D_g(F(x_i^s))) \quad (5)$$

$$\mathcal{L}_{global_t} = -\frac{1}{n_t} \sum_{i=1}^{n_t} D_g(F(x_i^t))^\gamma \log(1 - D_g(F(x_i^t))) \quad (6)$$

$$\mathcal{L}_{global}(F, D_g) = \frac{1}{2}(\mathcal{L}_{global_s} + \mathcal{L}_{global_t}) \quad (7)$$

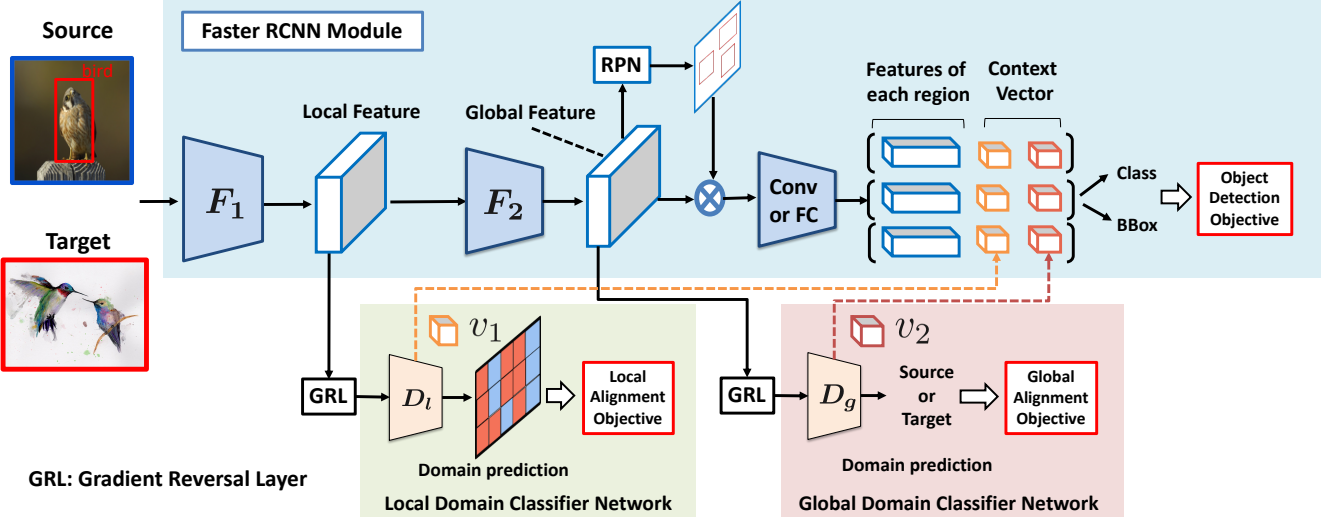


Figure 3. Proposed Network Architecture. Our method performs strong-local alignment by a local domain classifier network and weak-global alignment by a global domain classifier. The context vector is extracted by the domain classifiers and is concatenated in the layer before the final fully connected layer.

where n_t denotes the number of target examples.

The gradients of this loss should change the parameters of low-level layers, which should also align low-level features, but the effect may not be strong enough. We thus propose to directly perform the alignment in local-level features in the next sub-section.

3.2. Strong Local Feature Alignment

The architecture of the local domain classifier, D_l , is designed to focus on the local features rather than global features. D_l is a fully-convolutional network with kernel-size equal to one. The feature extractor F is decomposed as $F_2 \circ F_1$ and the output of F_1 is the input to D_l as shown in Fig. 3. F_1 outputs a feature whose width and height is W and H respectively. D_l outputs a domain prediction map which has the same width and height as the input feature. We employed a least-squares loss to train the domain classifier following [26, 42]. This loss function stabilizes the training of the domain classifier and is empirically shown to be useful for aligning low-level features. The loss function of the strong local alignment \mathcal{L}_{loc} is summarized as

$$\mathcal{L}_{loc_s} = \frac{1}{n_s H W} \sum_{i=1}^{n_s} \sum_{w=1}^W \sum_{h=1}^H D_l(F_1(x_i^s))_{wh}^2 \quad (8)$$

$$\mathcal{L}_{loc_t} = \frac{1}{n_t H W} \sum_{i=1}^{n_t} \sum_{w=1}^W \sum_{h=1}^H (1 - D_l(F_1(x_i^t))_{wh})^2 \quad (9)$$

$$\mathcal{L}_{loc}(F, D_l) = \frac{1}{2} (\mathcal{L}_{loc_s} + \mathcal{L}_{loc_t}) \quad (10)$$

where $D_l(F_1(x_i^s))_{wh}$ denotes the output of the domain classifier in each location. The loss is designed to align each

receptive field of features with the other domain.

3.3. Context Vector based Regularization

We further propose a regularization technique to improve the performance of our model. As discussed above, regularizing the domain classifier with the segmentation loss was effective for stabilizing the adversarial training in domain adaptive segmentation [35]. The authors designed a domain classifier that outputs both the domain label and a semantic segmentation map. Motivated by this approach, we propose to stabilize the training of the domain classifier by the detection loss computed on source examples. We extract vectors v_1 and v_2 from the middle layers of the two domain classifiers respectively. These vectors should contain information about whole input image, which is we call ‘‘context’’. Then, we concatenate the vectors with all region-wise features as shown in Fig. 3 and train the domain classifiers to minimize the detection loss on source examples as well as minimizing domain classification loss. During the test phase, the vectors are forwarded to obtain outputs.

3.4. Overall Objective

We denote the objective of detection modules as \mathcal{L}_{det} , which contains the loss for region proposal networks and final classification and localization error. The adversarial loss $\mathcal{L}_{adv}(F, D)$ is summarized as,

$$\mathcal{L}_{adv}(F, D) = \mathcal{L}_{loc}(F_1, D_l) + \mathcal{L}_{global}(F, D_g) \quad (11)$$

Combined with the loss of detection on source examples, the overall objective is,

$$\max_D \min_{F, R} \mathcal{L}_{cls}(F, R) - \lambda \mathcal{L}_{adv}(F, D) \quad (12)$$

Table 1. Results on adpatation from PASCAL VOC to Clipart Dataset. Average precision (%) is evaluated on target images. G, I, CTX, L indicate global alignment, instance-level alignment, context-vector based regularization, and local-alignment respectively.

| Method | G | I | CTX | L | aero | bicycle | bird | boat | bottle | bus | car | cat | chair | cow | table | dog | hrs | bike | prsn | plnt | sheep | sofa | train | tv | MAP |
|-------------|---|---|-----|---|-------------|-------------|-------------|-------------|-------------|-------------|-------------|-------------|-------------|-------------|-------------|-------------|-------------|-------------|-------------|-------------|-------------|-------------|-------------|-------------|-------------|
| Source Only | | | | | 35.6 | 52.5 | 24.3 | 23.0 | 20.0 | 43.9 | 32.8 | 10.7 | 30.6 | 11.7 | 13.8 | 6.0 | 36.8 | 45.9 | 48.7 | 41.9 | 16.5 | 7.3 | 22.9 | 32.0 | 27.8 |
| BDC-Faster | ✓ | | | | 20.2 | 46.4 | 20.4 | 19.3 | 18.7 | 41.3 | 26.5 | 6.4 | 33.2 | 11.7 | 26.0 | 1.7 | 36.6 | 41.5 | 37.7 | 44.5 | 10.6 | 20.4 | 33.3 | 15.5 | 25.6 |
| DA-Faster | ✓ | ✓ | | | 15.0 | 34.6 | 12.4 | 11.9 | 19.8 | 21.1 | 23.2 | 3.1 | 22.1 | 26.3 | 10.6 | 10.0 | 19.6 | 39.4 | 34.6 | 29.3 | 1.0 | 17.1 | 19.7 | 24.8 | 19.8 |
| Proposed | ✓ | | | | 30.5 | 48.5 | 33.6 | 24.8 | 41.2 | 48.9 | 32.4 | 17.2 | 34.5 | 55.0 | 19.0 | 13.6 | 35.1 | 66.2 | 63.0 | 45.3 | 12.5 | 22.6 | 45.0 | 38.9 | 36.4 |
| | ✓ | ✓ | | | 31.7 | 55.2 | 30.9 | 26.8 | 43.4 | 47.5 | 40.0 | 7.9 | 36.7 | 50.0 | 14.3 | 18.0 | 29.2 | 68.1 | 62.3 | 50.4 | 13.4 | 24.5 | 54.2 | 45.8 | 37.5 |
| | ✓ | ✓ | ✓ | | 26.2 | 48.5 | 32.6 | 33.7 | 38.5 | 54.3 | 37.1 | 18.6 | 34.8 | 58.3 | 17.0 | 12.5 | 33.8 | 65.5 | 61.6 | 52.0 | 9.3 | 24.9 | 54.1 | 49.1 | 38.1 |

Table 2. Results on PASCAL VOC in adaptation from PASCAL VOC to Clipart Dataset. Average precision (%) is evaluated on PASCAL. Our method does not degrade the performance on the source whereas BDC-Faster and DC-Faster degrade it.

| Method | G | I | CTX | L | MAP |
|-------------|---|---|-----|---|-------------|
| Source Only | | | | | 77.5 |
| BDC-Faster | ✓ | | | | 73.6 |
| DA-Faster | ✓ | ✓ | | | 66.4 |
| | ✓ | | | | 78.0 |
| Proposed | ✓ | ✓ | | | 77.6 |
| | ✓ | ✓ | ✓ | | 77.0 |

where λ controls the trade-off between detection loss and adversarial training loss. The sign of gradients is flipped by a gradient reversal layer proposed by [9]. Each mini-batch has one labeled source and one unlabeled target example.

4. Experiments

We evaluate our approach on four domain shifts—PASCAL [8] to Clipart [15], PASCAL to Watercolor [15], Cityscapes [6] to FoggyCityscapes [34], and GTA [17] to Cityscapes—to demonstrate that it is effective for adaptation between both dissimilar and similar domains. Additionally, we provide experiments to verify our claim that complete feature matching can degrade the performance of the model in the target domain.

Implementation Details. In all experiments, we set the shorter side of the image to 600 following the implementation of Faster RCNN [30] with ROI-alignment [12]. We first trained the networks with learning rate 0.001 for 50K iterations, then with learning rate 0.0001 for 20K more iterations and reported the final performance. All models are trained with this scheduling and we reported the performance trained after 70K iterations. Without specific notation, we set λ as 1.0 and γ as 5.0. We implemented all methods with Pytorch [28]. Please see our supplemental material for the detail of the network architecture.

We compared our method with three baselines: FRCNN model, FRCNN with a baseline domain classifier, and domain adaptive FRCNN (DA-Faster) [5]. FRCNN model was trained only on source examples without any adaptation. The FRCNN with a baseline domain classifier has

exactly the same architecture as our proposed weak-global alignment model, but its domain classifier is trained with cross-entropy loss in Eq. 5 and 6. The model does not have a local-level domain classifier. By comparing with this model, we can directly observe the effectiveness of our proposed weak alignment approach. Hereafter, we call the baseline *BDC-Faster*. *DA-Faster* [5] employs two domain classifiers, an image-level one for high-level features and an instance-level one for features cropped by the region proposal network. Both domain classifiers are trained by cross-entropy loss. In addition, it utilizes a technique called consensus regularization, which makes the outputs of two domain classifiers similar. Since we did not observe any benefit of the technique, we report the results without the technique. Since we implemented the method ourselves and the authors reported the best results during training, the results reported in the original paper and in our paper are slightly different.

4.1. Adaptation between dissimilar domains

We first show experiments on dissimilar domains, specifically, adaptation from real images to artistic images. We utilized the Pascal VOC Dataset as the real source domain [8]. This dataset contains 20 classes of images and their bounding box annotations. Following a prevalent evaluation protocol, we employed PASCAL VOC 2007 and 2012 training and validation splits for training, resulting in about 15k images. The target domain consists of either the Clipart or the Watercolor datasets [15]. Clipart contains comical images whereas Watercolor has artistic images. Clipart contains 1K images in total, which have the same 20 categories as PASCAL VOC.

All images were used for both training (without labels) and testing. Watercolor contains 6 categories in common with PASCAL and 2K images in total. 1K training images were utilized during training and our model is evaluated on 1K test images.

In this experiment, we used the ResNet101 [13] pre-trained on [7] as a backbone network. For other details see our supplemental material.

Results on Clipart. As shown in Table 1, our proposed method outperformed all baselines. Just by replacing the domain classifier’s objective with the focal loss, MAP im-

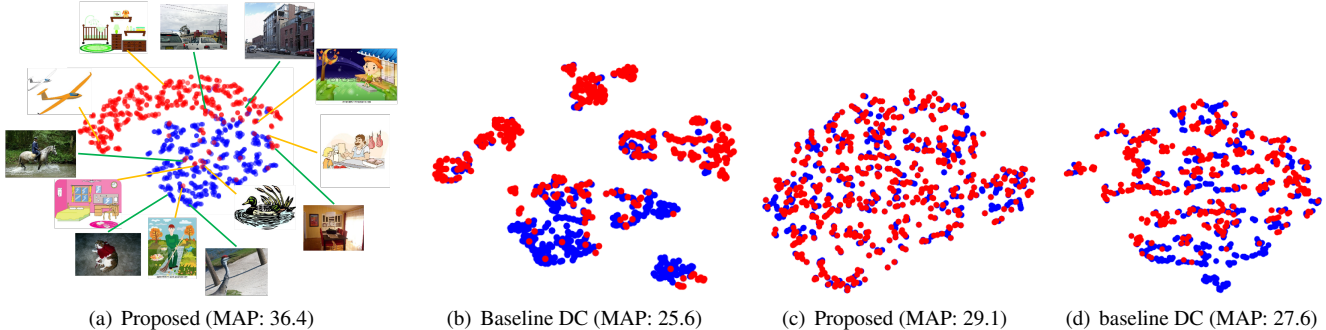


Figure 4. Visualization of features obtained by two different models. Blue: source examples, Red: target examples. Fig. (a) and (b) are the results of adaptation between dissimilar domains (from pascal to clipart). For Fig. (a), images with green lines are from PASCAL VOC (source). Images with orange lines are from Clipart (target). Our method does not match feature distributions strictly whereas the baseline method matches. However, our method outperformed the baseline with a large margin, which demonstrates the effectiveness of global-weak alignment. Fig. (d) and (c) are adaptation between similar domains (from Cityscape to FoggyCityscape). When the domains are very similar, the baseline method works well though our method performs better.

proved by 10.8% (25.6 to 36.4). In addition, the context vector based regularization and local alignment (C, L in Table), further improved MAP. The performance on the source domain, PASCAL VOC, is shown in Table 7. Compared with the performance of the source only model, BDC-Faster and DA-Faster significantly decrease its performance. This fact indicates that strictly aligning feature distributions between different domains can disturb the training for object detection while our method does not degrade the performance on the source domain.

We further visualized the features obtained by two models, our proposed global-level adaptation model and BDC-Faster in Fig. 4(a) and 4(b). The target features obtained by a baseline domain classifier are matched compactly with the source domain (Fig. 4(b)). On the other hand, with our proposed method (Fig. 4(a)), some features are aligned with the source features, but most of them are separated from source features. Source images usually focus on one or two objects whereas target images usually contain multiple images. Some target images focusing on single object are likely to be aligned with source as shown in the figure. Many existing methods for image classification aimed to match the feature distributions closely. However, this visualization implies that such distribution matching does not always help domain adaptive object detection.

Results on Watercolor. According to Table 3, our method outperformed the baseline methods. There was a large improvement on this domain. The improvement by the local alignment is especially large, about 3%, because the target images have a characteristic ‘‘painting’’ style. Therefore, the reducing the domain-gap based on local-level features improves the performance.

Table 3. AP on adpatation from PASCAL VOC to WaterColor (%). The definition of G, I, CTX, L is following Table 1.

| Method | G | I | CTX | L | AP on a target domain | | | | | | |
|-------------|---|---|-----|---|-----------------------|-------------|-------------|-------------|-------------|-------------|-------------|
| | | | | | bike | bird | car | cat | dog | prsn | MAP |
| Source Only | | | | | 68.8 | 46.8 | 37.2 | 32.7 | 21.3 | 60.7 | 44.6 |
| BDC-Faster | ✓ | | | | 68.6 | 48.3 | 47.2 | 26.5 | 21.7 | 60.5 | 45.5 |
| DA-Faster | ✓ | ✓ | | | 75.2 | 40.6 | 48.0 | 31.5 | 20.6 | 60.0 | 46.0 |
| Proposed | ✓ | | | | 66.4 | 53.7 | 43.8 | 37.9 | 31.9 | 65.3 | 49.8 |
| | ✓ | ✓ | | | 71.3 | 52.0 | 46.6 | 36.2 | 29.2 | 67.3 | 50.4 |
| | ✓ | ✓ | ✓ | ✓ | 82.3 | 55.9 | 46.5 | 32.7 | 35.5 | 66.7 | 53.3 |

Table 4. AP on adaptation from Cityscape to FoggyCityscape (%). The performance of our method is very near to oracle, which is trained on labeled target images.

| Method | G | I | CTX | L | AP on a target domain | | | | | | | |
|-------------|---|---|-----|---|-----------------------|-------------|-------------|-------------|-------------|-------------|-------------|-------------|
| | | | | | bus | bicycle | car | bike | prsn | rider | train | truck |
| Faster RCNN | | | | | 22.3 | 26.5 | 34.3 | 15.3 | 24.1 | 33.1 | 3.0 | 4.1 |
| BDC-Faster | ✓ | | | | 25.0 | 31.0 | 40.5 | 22.1 | 35.3 | 20.2 | 20.0 | 27.1 |
| DA-Faster | ✓ | ✓ | | | 33.1 | 23.3 | 25.5 | 15.6 | 23.4 | 29.0 | 10.9 | 19.6 |
| Proposed | ✓ | | | | 33.5 | 33.3 | 42.7 | 22.2 | 27.1 | 40.3 | 11.6 | 22.3 |
| | ✓ | ✓ | | | 34.3 | 32.2 | 36.2 | 23.7 | 27.5 | 39.3 | 5.4 | 24.4 |
| | ✓ | ✓ | ✓ | ✓ | 38.0 | 31.2 | 41.8 | 20.7 | 26.6 | 37.6 | 19.7 | 20.5 |
| Oracle | | | | | 36.2 | 35.3 | 43.5 | 30.0 | 29.9 | 42.3 | 32.6 | 24.5 |
| | | | | | | | | | | | | 34.3 |

4.2. Adaptation between similar domains

In this experiment, we aim to analyze our method by evaluating the adaptation between very similar domains. We used Cityscape [6] as the source domain. The images in the dataset are captured by a car-mounted video camera. As the target domain, we used FoggyCityscape datasets [34]. The images are rendered from Cityscape using depth information and it simulates the change of weather condition. The important difference from other adaptation scenario is that source and target images are originally the same one. Target images are generated from source images

Table 5. Results on adaptation from Sim10k to Cityscape Dataset (%). Average precision is evaluated on target images. FL ($\gamma = 3$)* indicates the experiments in which shorter side of image is scaled to 1000 during training and testing. P indicates pixel-level alignment, whether we used images generated by cyclegan during training. † indicates the performance when the context vector is zero-padded and not used for the output.

| Method | G | I | CTX | L | P | AP on Car |
|---|---|---|-----|---|---|--------------|
| Faster RCNN | | | | | | 34.6 |
| BDC-Faster | ✓ | | | | | 31.8 |
| DA-Faster | ✓ | ✓ | | | | 34.2 |
| Weak Align | ✓ | ✓ | | | | 35.8 |
| Proposed (FL) | | | | | | 36.4 |
| Proposed (FL) | | | | | | 38.2 (38.3)† |
| Proposed (FL) | | | | | | 40.1 |
| Proposed (FL) | | | | | | 41.5 |
| Proposed (FL) | | | | | | 40.7 |
| Proposed Method with different parameters | | | | | | |
| EFL | ✓ | | ✓ | | | 38.7 |
| FL ($\gamma = 3$) | ✓ | | ✓ | | | 42.3 |
| FL ($\gamma = 3$)* | ✓ | | ✓ | | ✓ | 47.7 |
| Oracle | | | | | | 53.1 |

by adding fog noise. In such adaptation scenario, strictly aligning feature distributions should be effective because there exists a correct matching between source and target images. Both dataset have 2, 975 images in the training set, and 500 images in the validation set. We utilized the training set during training and evaluated on the validation set. Since Cityscapes dataset does not have bounding-box annotation, we take the tightest rectangles of its instance masks as groundtruth bounding boxes. In this experiment, we used the VGG16 model [37] as a backbone network following [5].

As shown in Table 11, our proposed method performed much better than the baseline methods. MAP of a model with only strong local alignment was 27.9. Combining strong local and weak global alignment boosted MAP to 34.3. The domain-shift is caused by fog noise, a local-level shift. Hence, strong local alignment largely contributed to the improvement. In this adaptation scenario, the method with a baseline domain classifier performs much better than the source only model. This is because the target images have exactly the same layout and number/combination of objects. Thus, strongly aligning global features between different domains was effective. The visualized features in Fig. 4 show completely different characteristics from the experiments on PASCAL to Clipart dataset. The features are matched in both methods. The results indicate that our proposed method performs both when two domains are dissimilar and similar.

4.3. Adaptation from synthetic to real images

Here, we evaluate the performance of our model in an adaptation from synthetic images to real images. As the

synthetic domain, we used Sim10k [17] dataset. The dataset contains images of the synthetic driving scene, 10,000 training images which are collected from the computer game Grand Theft Auto (GTA). We employed the same architecture as used in the previous section. Following the protocol of [5], we evaluated detection performance on *car*. As a real domain, we used Cityscape dataset. All training images are used during training for both domains. Average precision was evaluated on the validation split of the Cityscape. We set the value of $\lambda = 0.1$ following [5] in Eq. 12. We show the performance when varying the value of λ in our supplemental material, where our method constantly performed better than a baseline. The two domains have similar layout in that both domains are driving scene images. However, the color and lighting are clearly different. In this respect, the two domains are more different than Cityscape and Fog-cityscape are. We extensively evaluated our method by ablating some components. Moreover, we show the results using instance-level adaptation as proposed in [5]. We also show the comparison and results of combination with a model trained with images translated by CycleGAN [42]. We trained CycleGAN to translate different domains’ images, then utilized the translated source images for training. Whether we employed the translated images is denoted by the column of P in Table 12. The details are shown in supplemental material. In addition, we demonstrate that our idea of weak alignment can be achieved with a loss function other than focal loss. In Eq. 2, we set $f(p_t) = e^{-\eta p_t}$, which is a decreasing function with the value of p_t . We call the loss function exponential focal loss (EFL). We set $\eta = 5.0$.

The results are summarized in Table 12. Our method constantly performed better than the baseline models. Comparing the results of BDC-Faster (31.8) and our method with only global-level alignment (36.4), the weak feature distribution alignment outperformed the strict alignment. Setting the value of $\gamma = 3.0$ in Focal Loss significantly improved the performance. In addition, with regard to a model trained with EFL, we could observe the improvement over the baseline models. The results demonstrate that our idea of weak global alignment is effective and can be achieved by functions other than Focal Loss.

Context vector based regularization and local-level alignment further improved the performance. The performance did not degrade when we did not use the context vector in test phase as seen in the table. This implies that the network does not use the vector for the prediction whereas the performance improved compared to the model without the regularization. Therefore, the context vector seems to contribute to the regularization of the domain classifier.

We could not see a positive effect of instance-level adaptation (Weak Align in Table 12). Instance-level alignment utilizes the cropped features by region proposal networks,

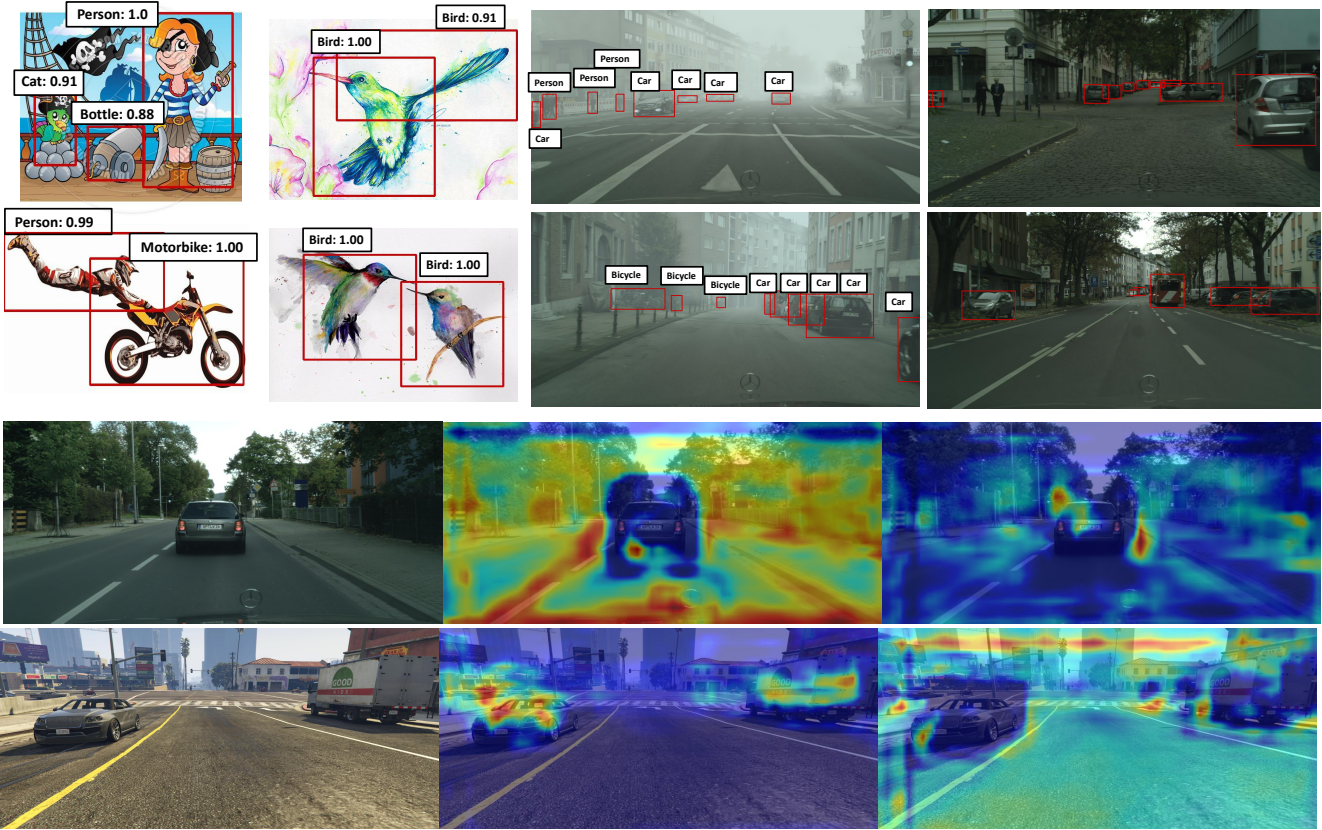


Figure 5. Upper: Examples of detection results on the target domain. From left to right column, Clipart, Watercolor, FoggyCityscape and Cityscape dataset. Bottom: Visualization of domain evidence using Grad-Cam. The evidence is obtained by the global-domain classifier. The pictures show results on target and source images respectively. Top images are target and bottom are source. From left to right, real images, images of evidence for the target, evidence of the source domain. Feature extractor seems to focus on deceiving the domain classifier in regions with car.

but the proposals may not localize objects in the target domain well, so it can hurt the performance of the model.

4.4. Analysis

Examples of detection results. We show the examples of detection results in Fig. 5. Even when the style of the images is different between the source and target, our model localizes objects correctly in these cases. As seen in Clipart’s example, when the appearance of the objects is largely different, the detection results are not successful. Also, as seen in case of Watercolor, the detector tends to output multiple predictions to one object. In case of FoggyCityscape’s examples, our model tends to assign one bounding box to multiple neighboring bicycles.

Visualization of domain evidence. To analyze the behavior of the feature extractor and domain classifier, we visualize the evidence for the global-level domain classifier’s prediction using Grad-cam [36] in Fig. 5. We use Grad-cam to show the evidence (heatmap) for why the domain classifier thinks the image comes from the source or the target, for the adaptation from Sim10k to Cityscapes. Please see

our supplemental material for other examples. For the target images, the domain classifier does not look at cars as the evidence for the target. Similarly, for source images, it also does not look at cars as the evidence for the source. This indicates that the feature extractor seems to focus on cars to deceive the domain classifier, which means that the feature extractor learns to partially align global-image features, specifically around cars.

5. Conclusion

In this work, we propose a novel approach for detector adaptation based on strong local alignment and weak global alignment for unsupervised adaptation of object detectors. Our key contribution is the weak alignment model, which focuses the adversarial alignment loss on images that are globally similar and puts less emphasis on aligning images that are globally dissimilar. Additionally, we design the strong domain alignment model to only look at local receptive fields of the feature map. Our method outperformed other existing methods with a large-margin in several datasets. Through extensive experiments, we verified

the effectiveness of weak global and strong local alignment.

6. Acknowledgement

This work was supported by Honda, DARPA and NSF. It was partially supported by JST CREST Grant Number JPMJCR1403, Japan.

References

- [1] S. Ben-David, J. Blitzer, K. Crammer, A. Kulesza, F. Pereira, and J. W. Vaughan. A theory of learning from different domains. *Machine learning*, 79(1-2):151–175, 2010. [1](#) [2](#)
- [2] S. Ben-David, J. Blitzer, K. Crammer, F. Pereira, et al. Analysis of representations for domain adaptation. In *NIPS*, 2007. [1](#) [2](#)
- [3] H. Bilen and A. Vedaldi. Weakly supervised deep detection networks. In *CVPR*, 2016. [2](#)
- [4] P. P. Busto and J. Gall. Open set domain adaptation. In *ICCV*, 2017. [1](#)
- [5] Y. Chen, W. Li, C. Sakaridis, D. Dai, and L. Van Gool. Domain adaptive faster r-cnn for object detection in the wild. In *CVPR*, 2018. [2](#) [3](#) [5](#) [7](#)
- [6] M. Cordts, M. Omran, S. Ramos, T. Rehfeld, M. Enzweiler, R. Benenson, U. Franke, S. Roth, and B. Schiele. The cityscapes dataset for semantic urban scene understanding. In *CVPR*, 2016. [5](#) [6](#)
- [7] J. Deng, W. Dong, R. Socher, L.-J. Li, K. Li, and L. Fei-Fei. Imagenet: A large-scale hierarchical image database. In *CVPR*. [2](#) [5](#)
- [8] M. Everingham, L. Van Gool, C. K. Williams, J. Winn, and A. Zisserman. The pascal visual object classes (voc) challenge. *IJCV*, 88(2):303–338, 2010. [2](#) [5](#)
- [9] Y. Ganin and V. Lempitsky. Unsupervised domain adaptation by backpropagation. In *ICML*, 2014. [2](#) [5](#)
- [10] Y. Ganin, E. Ustinova, H. Ajakan, P. Germain, H. Larochelle, F. Laviolette, M. Marchand, and V. Lempitsky. Domain-adversarial training of neural networks. *JMLR*, 17(59):1–35, 2016. [1](#)
- [11] I. Goodfellow, J. Pouget-Abadie, M. Mirza, B. Xu, D. Warde-Farley, S. Ozair, A. Courville, and Y. Bengio. Generative adversarial nets. In *NIPS*, 2014. [2](#)
- [12] K. He, G. Gkioxari, P. Dollár, and R. Girshick. Mask r-cnn. In *ICCV*, 2017. [5](#)
- [13] K. He, X. Zhang, S. Ren, and J. Sun. Deep residual learning for image recognition. In *CVPR*, 2016. [5](#)
- [14] J. Hoffman, E. Tzeng, T. Park, J.-Y. Zhu, P. Isola, K. Saenko, A. A. Efros, and T. Darrell. Cycada: Cycle-consistent adversarial domain adaptation. In *ICML*, 2018. [1](#)
- [15] N. Inoue, R. Furuta, T. Yamasaki, and K. Aizawa. Cross-domain weakly-supervised object detection through progressive domain adaptation, 2018. [5](#)
- [16] Y. Jia, E. Shelhamer, J. Donahue, S. Karayev, J. Long, R. Girshick, S. Guadarrama, and T. Darrell. Caffe: Convolutional architecture for fast feature embedding. In *ACMMM*. ACM, 2014. [11](#)
- [17] M. Johnson-Roberson, C. Barto, R. Mehta, S. N. Sridhar, K. Rosaen, and R. Vasudevan. Driving in the matrix: Can virtual worlds replace human-generated annotations for real world tasks? *arXiv preprint arXiv:1610.01983*, 2016. [5](#) [7](#)
- [18] A. Krizhevsky, I. Sutskever, and G. E. Hinton. Imagenet classification with deep convolutional neural networks. In *NIPS*, 2012. [1](#)
- [19] T.-Y. Lin, P. Goyal, R. Girshick, K. He, and P. Dollár. Focal loss for dense object detection. In *ICCV*, 2017. [3](#)
- [20] T.-Y. Lin, M. Maire, S. Belongie, J. Hays, P. Perona, D. Ramanan, P. Dollár, and C. L. Zitnick. Microsoft coco: Common objects in context. In *ECCV*, 2014. [2](#)
- [21] M.-Y. Liu, T. Breuel, and J. Kautz. Unsupervised image-to-image translation networks. In *NIPS*, 2017. [1](#)
- [22] W. Liu, D. Anguelov, D. Erhan, C. Szegedy, S. Reed, C.-Y. Fu, and A. C. Berg. Ssd: Single shot multibox detector. In *ECCV*, 2016. [2](#)
- [23] M. Long, Y. Cao, J. Wang, and M. I. Jordan. Learning transferable features with deep adaptation networks. In *ICML*, 2015. [2](#)
- [24] M. Long, Z. Cao, J. Wang, and M. I. Jordan. Conditional adversarial domain adaptation. In *NIPS*, 2018. [2](#)
- [25] M. Long, H. Zhu, J. Wang, and M. I. Jordan. Unsupervised domain adaptation with residual transfer networks. In *NIPS*, 2016. [1](#) [2](#)
- [26] X. Mao, Q. Li, H. Xie, R. Y. Lau, Z. Wang, and S. P. Smolley. Least squares generative adversarial networks. In *ICCV*, 2017. [4](#)
- [27] A. Odena, C. Olah, and J. Shlens. Conditional image synthesis with auxiliary classifier gans, 2017. [3](#)
- [28] A. Paszke, S. Gross, S. Chintala, G. Chanan, E. Yang, Z. DeVito, Z. Lin, A. Desmaison, L. Antiga, and A. Lerer. Automatic differentiation in pytorch. 2017. [5](#)
- [29] J. Redmon, S. Divvala, R. Girshick, and A. Farhadi. You only look once: Unified, real-time object detection. In *CVPR*, 2016. [2](#)
- [30] S. Ren, K. He, R. Girshick, and J. Sun. Faster r-cnn: Towards real-time object detection with region proposal networks. In *NIPS*, 2015. [2](#) [5](#)
- [31] K. Saenko, B. Kulis, M. Fritz, and T. Darrell. Adapting visual category models to new domains. In *ECCV*, 2010. [1](#) [2](#)
- [32] K. Saito, Y. Ushiku, T. Harada, and K. Saenko. Adversarial dropout regularization. In *ICLR*, 2018. [1](#)
- [33] K. Saito, K. Watanabe, Y. Ushiku, and T. Harada. Maximum classifier discrepancy for unsupervised domain adaptation. In *CVPR*, 2018. [2](#)
- [34] C. Sakaridis, D. Dai, and L. Van Gool. Semantic foggy scene understanding with synthetic data. *IJCV*, 2018. [5](#) [6](#)
- [35] S. Sankaranarayanan, Y. Balaji, A. Jain, S. N. Lim, and R. Chellappa. Learning from synthetic data: Addressing domain shift for semantic segmentation. In *CVPR*, 2018. [2](#) [3](#) [4](#)
- [36] R. R. Selvaraju, M. Cogswell, A. Das, R. Vedantam, D. Parikh, D. Batra, et al. Grad-cam: Visual explanations from deep networks via gradient-based localization. In *ICCV*, 2017. [8](#)

- [37] K. Simonyan and A. Zisserman. Very deep convolutional networks for large-scale image recognition. *arXiv preprint arXiv:1409.1556*, 2014. 7
- [38] Y. Tang, J. Wang, B. Gao, E. Dellandr  , R. Gaizauskas, and L. Chen. Large scale semi-supervised object detection using visual and semantic knowledge transfer. In *CVPR*, 2016. 2
- [39] E. Tzeng, J. Hoffman, K. Saenko, and T. Darrell. Adversarial discriminative domain adaptation. In *CVPR*, 2017. 1, 2
- [40] E. Tzeng, J. Hoffman, N. Zhang, K. Saenko, and T. Darrell. Deep domain confusion: Maximizing for domain invariance. *arXiv:1412.3474*, 2014. 1, 2
- [41] J. Zhang, Z. Ding, W. Li, and P. Ogunbona. Importance weighted adversarial nets for partial domain adaptation. In *CVPR*, 2018. 1
- [42] J.-Y. Zhu, T. Park, P. Isola, and A. A. Efros. Unpaired image-to-image translation using cycle-consistent adversarial networks. *ICCV*, 2017. 4, 7
- [43] Y. Zou, Z. Yu, B. V. Kumar, and J. Wang. Unsupervised domain adaptation for semantic segmentation via class-balanced self-training. In *ECCV*, 2018. 2

Supplemental Material

1. Network Architecture

We used the same architecture of the domain classifier for Faster RCNN with ResNet101 and VGG16. As the number of the channels in input features is different, we changed the channel size of network according to the backbone network.

In case of VGG16 model, the feature in *conv3_3* layer is fed into the local domain classifier. The feature in the last *res2c* layer is fed into the local domain classifier with regard to ResNet101 model. The name of the layer is cited by the Caffe [16] prototxt.

Table 6. The architecture of the domain classifiers.

| Global Domain Classifier | Local Domain Classifier |
|--|--|
| Conv $3 \times 3 \times 512$, stride 2, pad 1 | Conv $1 \times 1 \times 256$, stride 1, pad 0 |
| Batch Normalization, ReLU, Dropout | ReLU |
| Conv $3 \times 3 \times 128$, stride 2, pad 1 | Conv $1 \times 1 \times 128$, stride 1, pad 0 |
| Batch Normalization, ReLU, Dropout | ReLU |
| Conv $3 \times 3 \times 128$, stride 2, pad 1 | Conv $1 \times 1 \times 1$, stride 1, pad 0 |
| Batch Normalization, ReLU, Dropout | Sigmoid |
| Average Pooling | |
| Fully connected 128×2 | |
| Softmax | |

Global Domain Classifier

The global domain classifier have three layered convolution layers, global average pooling and one Linear layer. The kernel size of the convolution layers is set as three. Batch Normalization, ReLU, and dropout layers are attached after each convolution layers. The output of the global domain classifier is activated by softmax function. Context vector is extracted after the average pooling layer. Therefore, the vector has 128 dimension.

Local Domain Classifier

The local domain classifier have three layered convolution layers. The kernel size of the convolution layers is set as one. The output of the local domain classifier is activated by sigmoid function. Context vector is extracted before the last convolution layer. Therefore, the vector has 128 dimension.

2. Pixel-level Adaptation

The results on a model trained with images generated by CycleGAN were provided in our paper. We describe the detail of how we trained the model.

Training of CycleGAN

To train the CycleGAN, we used the Pytorch-implementation of the paper. We used all training images in both domains. We trained CycleGAN for 10 epochs and employed the source images translated into the target domain for training our Faster RCNN model.

Training of Faster RCNN

We found that some of the translated images are not translated correctly. Cars are completely hidden by large noise. In order to suppress the effect of such corrupted images, we trained our model using source, translated source and target images. Translated images are utilized just for training detection modules and not utilized for domain classification. Namely, we have three images in each mini-batch, source, translated source and target image. Source and target images are used as we mentioned in our main paper. The translated source one is used to calculate and backward the detection loss.

3. Additional Results

Results on source domain

Table 7, 10, and 11 show the results on source domain in three adaptation scenarios. In all scenarios, our method does not significantly degrade the detection performance on the source domain.

Results on target domain

Table 8, 10 and 12 provide results including local-level only adaptation and pixel-level adaptation. In adaptation for clipart dataset, training with the images generated by CycleGAN does not improve the performance. The possible reasons are that the style of the target images is largely different and that target images have diverse styles of examples. Then, CycleGAN may not generate images suitable for adaptive detection. In the experiments on Watercolor, the performance greatly improved

with the use of pixel-level adaptation. The model demonstrates almost oracle-level performance. Table 9 denotes the results when using VGG network for the adaptation from PASCAL VOC to clipart. The performance largely improved with our method.

Parameter Sensitivity

Fig. 6(a) presents the sensitivity to the parameter λ in Eq. 12 in our main paper. The parameter is the trade-off between training of detection and adversarial training. Our method performed better than the baseline domain classifier in all values ranging from 0 to 1.

Fig. 6(b) presents the sensitivity to the parameter γ of Focal Loss. The result is obtained in adaptation from Sim10k to Cityscape. The parameter controls how strictly we align features between domains. As the parameter gets small, the domain classifier will look at all examples. As shown in the figure, the peak of the performance was around 3.0, in which AP was 42.3.

Domain Evidence

Fig. 7 is the additional domain evidence visualization. Although the behavior differs from dataset to dataset, the domain classifier tries to find the evidence from either background or foreground objects.

Table 7. Results on PASCAL VOC in adaptation from PASCAL VOC to Clipart Dataset. Average precision (%) is evaluated on PASCAL. Our method does not degrade the performance on the source whereas BDC-Faster and DC-Faster degrade it.

| Method | G | I | C | L | aero | cycle | bird | boat | bottle | bus | car | cat | chair | cow | table | dog | hrs | bike | prsn | plnt | sheep | sofa | train | tv | MAP |
|-------------|---|---|---|---|-------------|-------------|-------------|-------------|-------------|-------------|-------------|-------------|-------------|-------------|-------------|-------------|-------------|-------------|-------------|-------------|-------------|-------------|-------------|-------------|-------------|
| Faster RCNN | | | | | 77.7 | 80.3 | 82.5 | 79.0 | 68.0 | 88.1 | 85.7 | 87.0 | 53.1 | 87.3 | 58.2 | 88.3 | 85.0 | 87.9 | 80.5 | 52.8 | 75.9 | 69.4 | 86.3 | 77.8 | 77.5 |
| BDC-Faster | ✓ | | | | 77.6 | 80.0 | 77.6 | 61.8 | 61.3 | 83.0 | 86.1 | 86.5 | 50.9 | 79.8 | 59.8 | 84.7 | 82.2 | 79.5 | 78.1 | 45.3 | 73.4 | 70.1 | 80.8 | 73.8 | 73.6 |
| DA-Faster | ✓ | ✓ | | | 64.5 | 70.6 | 66.4 | 62.9 | 49.9 | 77.2 | 78.0 | 70.7 | 44.7 | 78.3 | 56.1 | 70.8 | 75.6 | 85.2 | 74.5 | 37.2 | 65.4 | 60.2 | 72.3 | 66.9 | 66.4 |
| Proposed | | | | ✓ | 79.5 | 80.7 | 82.5 | 78.6 | 62.2 | 86.1 | 85.4 | 87.5 | 60.2 | 79.0 | 68.8 | 88.6 | 86.2 | 88.7 | 78.9 | 52.5 | 78.5 | 71.6 | 87.9 | 76.9 | 78.0 |
| | | ✓ | | | 78.6 | 81.7 | 83.4 | 74.7 | 62.9 | 86.9 | 85.4 | 90.6 | 56.8 | 85.7 | 57.9 | 89.0 | 87.4 | 87.7 | 78.1 | 52.3 | 79.3 | 67.6 | 87.6 | 79.5 | 77.6 |
| | | ✓ | ✓ | | 77.5 | 84.7 | 81.1 | 71.1 | 63.8 | 88.5 | 84.7 | 87.7 | 54.5 | 81.6 | 60.8 | 89.4 | 87.8 | 88.2 | 78.2 | 49.9 | 78.9 | 70.2 | 82.0 | 79.5 | 77.0 |

Table 8. Results on adaptation from PASCAL VOC to Clipart Dataset. Average precision (%) is evaluated on target images. G, I, CTX, L, P indicate global alignment, instance-level alignment, context-vector based regularization, local-alignment and pixel-alignment respectively. Faster RCNN \dagger indicates Faster RCNN trained by source images and translated source images by CycleGAN.

| Method | G | I | CTX | L | P | aero | cycle | bird | boat | bottle | bus | car | cat | chair | cow | table | dog | hrs | bike | prsn | plnt | sheep | sofa | train | tv | MAP |
|-----------------------|---|---|-----|---|---|-------------|-------------|-------------|-------------|-------------|-------------|-------------|-------------|-------------|-------------|-------------|-------------|-------------|-------------|-------------|-------------|-------------|-------------|-------------|-------------|-------------|
| Faster RCNN | | | | | | 35.6 | 52.5 | 24.3 | 23.0 | 20.0 | 43.9 | 32.8 | 10.7 | 30.6 | 11.7 | 13.8 | 6.0 | 36.8 | 45.9 | 48.7 | 41.9 | 16.5 | 7.3 | 22.9 | 32.0 | 27.8 |
| Faster RCNN \dagger | | | | | ✓ | 26.4 | 52.7 | 28.3 | 24.1 | 28.5 | 49.7 | 30.2 | 13 | 35.3 | 26.5 | 15.8 | 7.6 | 26.1 | 68.1 | 47.2 | 42.5 | 5.9 | 23.2 | 41 | 42.6 | 31.7 |
| BDC-Faster | ✓ | | | | | 20.2 | 46.4 | 20.4 | 19.3 | 18.7 | 41.3 | 26.5 | 6.4 | 33.2 | 11.7 | 26.0 | 1.7 | 36.6 | 41.5 | 37.7 | 44.5 | 10.6 | 20.4 | 33.3 | 15.5 | 25.6 |
| DA-Faster | ✓ | ✓ | | | | 15.0 | 34.6 | 12.4 | 11.9 | 19.8 | 21.1 | 23.2 | 3.1 | 22.1 | 26.3 | 10.6 | 10.0 | 19.6 | 39.4 | 34.6 | 29.3 | 1.0 | 17.1 | 19.7 | 24.8 | 19.8 |
| Proposed | | | | ✓ | | 30.5 | 48.5 | 33.6 | 24.8 | 41.2 | 48.9 | 32.4 | 17.2 | 34.5 | 55.0 | 19.0 | 13.6 | 35.1 | 66.2 | 63.0 | 45.3 | 12.5 | 22.6 | 45.0 | 38.9 | 36.4 |
| | | | | ✓ | | 19.8 | 50.7 | 25.4 | 21.7 | 30.2 | 47.2 | 27.1 | 8.5 | 33.5 | 26.8 | 14.0 | 11.7 | 31.5 | 62.0 | 49.9 | 39.6 | 9.1 | 23.8 | 39.5 | 38.4 | 30.5 |
| | ✓ | ✓ | | | | 31.7 | 55.2 | 30.9 | 26.8 | 43.4 | 47.5 | 40.0 | 7.9 | 36.7 | 50.0 | 14.3 | 18.0 | 29.2 | 68.1 | 62.3 | 50.4 | 13.4 | 24.5 | 54.2 | 45.8 | 37.5 |
| | ✓ | ✓ | ✓ | | | 26.2 | 48.5 | 32.6 | 33.7 | 38.5 | 54.3 | 37.1 | 18.6 | 34.8 | 58.3 | 17.0 | 12.5 | 33.8 | 65.5 | 61.6 | 52.0 | 9.3 | 24.9 | 54.1 | 49.1 | 38.1 |
| | ✓ | ✓ | ✓ | ✓ | | 31.1 | 53.7 | 28.9 | 24.9 | 40.3 | 49.0 | 38.1 | 14.6 | 41.9 | 43.8 | 15.3 | 7.2 | 27.9 | 75.5 | 57.3 | 41.8 | 6.7 | 23.3 | 48.5 | 44.1 | 35.7 |

Table 9. Results on adaptation from PASCAL VOC to Clipart Dataset with VGG. Average precision (%) is evaluated on target images.

| Method | G | CTX | L | P | aero | cycle | bird | boat | bottle | bus | car | cat | chair | cow | table | dog | hrs | bike | prsn | plnt | sheep | sofa | train | tv | MAP |
|-------------|---|-----|---|---|------|-------|------|------|--------|------|------|------|-------|------|-------|------|------|------|------|------|-------|------|-------|------|------|
| Faster RCNN | | | | | 15.7 | 31.9 | 22.4 | 8.2 | 38.8 | 59.4 | 17.8 | 6.6 | 37.0 | 5.7 | 12.7 | 7.2 | 17.4 | 49.0 | 36.0 | 32.1 | 11.2 | 2.9 | 29.8 | 28.4 | 23.5 |
| BDC-Faster | ✓ | | | | 11.0 | 40.9 | 12.2 | 10.1 | 28.9 | 29.2 | 28.0 | 6.0 | 23.5 | 8.8 | 13.1 | 6.5 | 22.4 | 45.6 | 46.9 | 35.9 | 9.7 | 9.3 | 18.9 | 20.9 | 21.4 |
| Proposed | ✓ | ✓ | | | 18.6 | 45.0 | 22.2 | 23.2 | 23.9 | 21.1 | 28.6 | 5.2 | 31.8 | 39.1 | 19.7 | 0.9 | 25.2 | 56.1 | 54.3 | 36.1 | 27.8 | 6.8 | 32.4 | 40.4 | 27.9 |
| | ✓ | ✓ | ✓ | | 16.0 | 53.2 | 27.5 | 21.6 | 32.0 | 48.4 | 32.4 | 12.2 | 32.5 | 27.3 | 12.3 | 13.1 | 24.3 | 62.4 | 55.5 | 41.2 | 21.0 | 13.2 | 37.8 | 46.1 | 31.5 |

Table 10. Results on adaptation from PASCAL VOC to WaterColor Dataset (%). Left: AP evaluated on PASCAL VOC. Right: AP evaluated on WaterColor. AP on adaptation from PASCAL VOC to WaterColor (%). The definition of G, I, CTX, L is the same as defined in the main paper. Faster RCNN \dagger indicates Faster RCNN trained by source images and translated source images by CycleGAN.

| Method | G | I | CTX | L | P | AP on a source domain | | | | | | AP on a target domain | | | | | | | | |
|-----------------------|---|---|-----|---|---|-----------------------|------|------|------|------|------|-----------------------|------|------|------|------|------|------|------|------|
| | | | | | | bike | bird | car | cat | dog | prsn | MAP | bike | bird | car | cat | dog | prsn | | |
| Faster RCNN | | | | | | 82.1 | 82.3 | 86.5 | 89.3 | 85.6 | 84.3 | 85.0 | 68.8 | 46.8 | 37.2 | 32.7 | 21.3 | 60.7 | 44.6 | |
| Faster RCNN \dagger | | | | | | ✓ | 79.7 | 82.7 | 86 | 88.9 | 85 | 82.1 | 84.1 | 83.3 | 52.7 | 45.3 | 33.1 | 28.8 | 64 | 51.2 |
| BDC-Faster | ✓ | | | | | 80.9 | 82.6 | 86.4 | 87.9 | 82.7 | 83.3 | 84.0 | 68.6 | 48.3 | 47.2 | 26.5 | 21.7 | 60.5 | 45.5 | |
| DA-Faster | ✓ | ✓ | | | | 75.7 | 84.4 | 84.5 | 88.5 | 83.6 | 81.6 | 83.1 | 75.2 | 40.6 | 48.0 | 31.5 | 20.6 | 60.0 | 46.0 | |
| Proposed | | | | | | ✓ | 79.4 | 84.6 | 85.8 | 89.6 | 85.7 | 84.1 | 84.9 | 66.4 | 53.7 | 43.8 | 37.9 | 31.9 | 65.3 | 49.8 |
| | | | | | | ✓ | 80.0 | 82.0 | 84.7 | 86.8 | 83.6 | 81.3 | 83.1 | 79.4 | 54.8 | 47.2 | 37.1 | 31.5 | 62.4 | 52.1 |
| | ✓ | ✓ | | | | 79.5 | 84.6 | 86.1 | 89.2 | 84.5 | 82.8 | 84.4 | 71.3 | 52.0 | 46.6 | 36.2 | 29.2 | 67.3 | 50.4 | |
| | ✓ | ✓ | ✓ | | | 79.8 | 87.4 | 85.5 | 88.1 | 84.5 | 84.0 | 84.9 | 82.3 | 55.9 | 46.5 | 32.7 | 35.5 | 66.7 | 53.3 | |
| | ✓ | ✓ | ✓ | ✓ | | 78.9 | 83.1 | 84.2 | 87.4 | 85.6 | 82.8 | 83.7 | 90.5 | 54.8 | 49.4 | 38.6 | 38.8 | 67.9 | 56.7 | |
| Oracle | | | | | | 82.1 | 82.3 | 86.5 | 89.3 | 85.6 | 84.3 | 85.0 | 83.6 | 59.4 | 50.7 | 43.7 | 39.5 | 74.5 | 58.6 | |

Table 11. Results on adaptation from Cityscape to FoggyCityscape Dataset (%). The performance is evaluated on Cityscape.

| Method | G | I | CTX | L | AP on a source domain | | | | | | | MAP | | |
|-------------|---|---|-----|---|-----------------------|-------|------|-------|------|-------|-------|-------|------|------|
| | | | | | bus | beycl | car | meycl | prsn | rider | train | truck | | |
| Faster RCNN | | | | | 55.6 | 39.0 | 52.3 | 38.8 | 33.7 | 47.7 | 39.1 | 33.1 | 42.4 | |
| NDC-Faster | ✓ | | | | 56.4 | 38.2 | 52.7 | 36.5 | 33.6 | 49.3 | 41.9 | 32.0 | 42.6 | |
| DA-Faster | ✓ | ✓ | | | 58.3 | 38.8 | 52.6 | 42.5 | 35.1 | 47.6 | 44.1 | 34.2 | 44.2 | |
| Proposed | | | | | ✓ | 62.6 | 37.9 | 52.2 | 35.1 | 35.0 | 48.5 | 47.7 | 34.9 | 44.2 |
| | ✓ | ✓ | | | 57.0 | 39.3 | 52.3 | 39.9 | 33.6 | 48.3 | 41.6 | 36.0 | 43.5 | |
| | ✓ | ✓ | ✓ | | 57.9 | 39.4 | 52.6 | 39.4 | 35.2 | 48.3 | 47.7 | 37.4 | 44.7 | |

Table 12. Results on adaptation from Sim10k to Cityscape Dataset (%). Average precision is evaluated on target images. Faster RCNN \dagger indicates Faster RCNN trained by source images and translated source images by CycleGAN.

| Method | G | I | CTX | L | P | AP on Car |
|---|---|---|-----|---|---|-----------|
| Faster RCNN | | | | | | 34.6 |
| Faster RCNN \dagger | | | | | ✓ | 40.0 |
| BDC-Faster | ✓ | | | | | 31.8 |
| DA-Faster | ✓ | ✓ | | | | 34.2 |
| Proposed (FL) | | | | | ✓ | 36.4 |
| | ✓ | ✓ | | | ✓ | 40.2 |
| | ✓ | ✓ | ✓ | | | 38.2 |
| | ✓ | ✓ | ✓ | ✓ | | 40.1 |
| | ✓ | ✓ | ✓ | ✓ | ✓ | 41.5 |
| Proposed Method with different parameters | | | | | | 40.7 |
| FL ($\gamma = 3$) | ✓ | ✓ | | | | 42.3 |
| Oracle | | | | | | 53.1 |

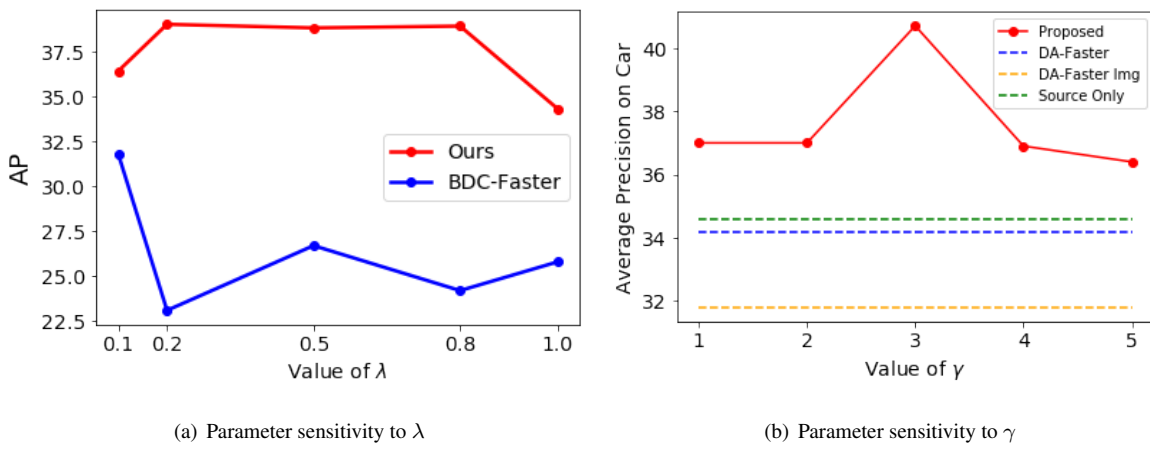


Figure 6. Parameter sensitivity to the value of λ (Left) and γ (Right) in adaptation from Sim10k to Cityscape.

Source Images



Target Images

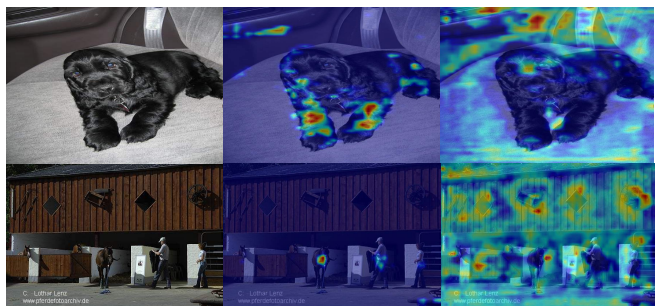
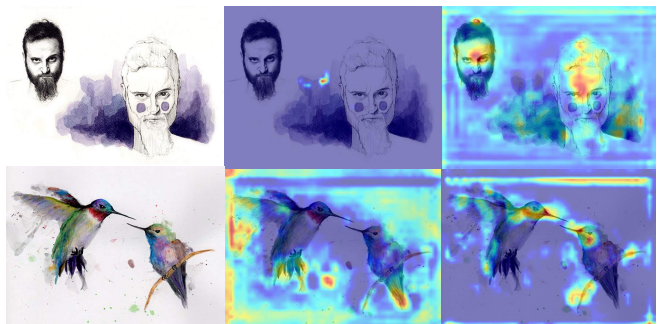
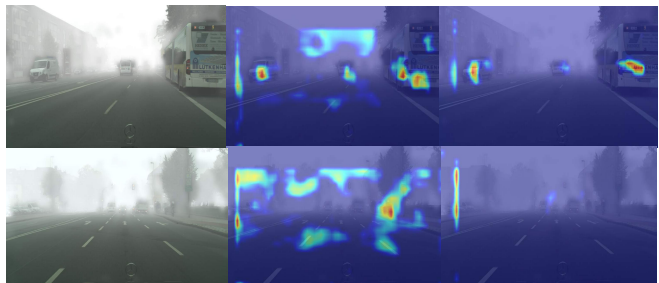
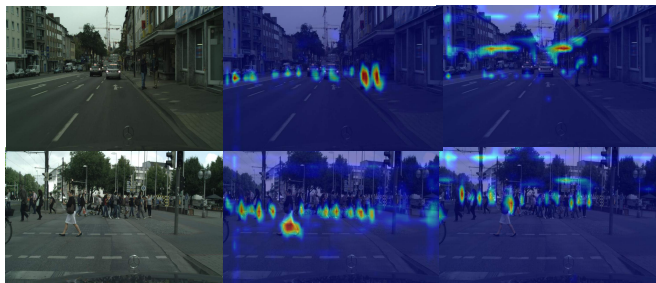


Figure 7. Visualization of domain evidence using Grad-Cam. The evidence is obtained by the global-domain classifier. The pictures show results on target and source images respectively. From left to right, real images, images of evidence for the target, evidence of the source domain. The behavior of the domain classifier seems to be different in the adaptation scenarios. However, the classifier tries to focus on foreground objects or background to find the evidence of the domain.